Chapter 6

Multiscaling of shear zones

C. Schrank, M.R. Handy and F. Fusseis[1]

6.1 Abstract

A new method is introduced for quantifying the scale and the intensity of strain localization from areal images of natural shear zones. The method employs Autocorrelation Functions (ACF) to determine local scales of geometric homogeneity, or elementary reference areas, for calculating scale-dependent localization factors of deformed rock. In a separate step, the intensity of strain localization is quantified from measurements of maximum shear strain relative to average or background shear strain. This approach is used to analyze shear zones on different scales (mm to km) from an exposure of the fossil brittle-viscous transition (BVT) at the Cap de Creus in NE Spain. Changes in the scaling characteristics of shear zones across this area are interpreted to reflect a time-sequence of localization during the evolution of the continental BVT. It is shown that the scales of strain localization are related partly to inherited anisotropies (older schistosity, sedimentary layering, pegmatite bodies) and partly to the predominant mode of deformation (brittle, viscous). The length-to-width ratio of shear zones decreases with scale as they evolved in time and space from isolated shear fractures to interconnected mylonitic shear zones. Variations of strain intensity calculated along a single shear zone indicate that such shear zones weakened from their brittle tips to

---

their mylonitic centers, thus driving their propagation and growth to larger scales. Our results support the notion that the BVT evolves by "upscaling", a process whereby strain localizes on progressively larger length scales until a dense network of weak, mylonitic layers some tens to hundreds of meters wide forms subparallel to the regional shearing plane.

6.2   Introduction

Rock deformation is observed to be homogeneous on some length scales and heterogeneous on others, but the determinants of these scales have remained enigmatic almost since the first detailed descriptions of rock deformation (eeg. Heim 1878 in Milnes 1979). This enigma has been compounded by the unresolved methodological challenge of quantifying deformational heterogeneity on the broad range of scales over which such heterogeneity occurs in Nature, from the width of mineral grains (microns-millimeters) to the length of plate-boundary faults ($10^2 - 10^4$km). Heterogeneous rock deformation on all these scales is manifested by discrete zones of displacement, termed shear zones, that are characterized by finite strain gradients both parallel and perpendicular to their length (Fig. 6.1, Ramsay 1980). At high strains, isolated shear zones link up to form a network of anastomosing shear zones that are oriented subparallel to the bulk shearing plane (Fig. 6.1a, e.g. Fusseis et al. 2006). The question arises of how such networks evolve in time and space, specifically whether the process of networking involves changes in the length scale of deformation. Following Handy et al. (in press), a network of shear zones is considered to evolve to a smaller length scale when strain is progressively localized into a narrow shear zone while surrounding shear zones are deactivated. This evolution is termed "down-scaling" because strain is localized in a smaller volume of rock than that of the initial shear zone array. On the other hand, the networking is said to involve "upscaling" if shearing affects progressively larger volumes of rock. The strain becomes more homogeneous as isolated shear zones widen and coalesce, leading to the formation of a shear zone that is larger than the initial shear zone array. Both upscaling and downscaling are viable processes, having been inferred for natural fault systems (upscaling: Fusseis et al., 2006, downscaling: Chester et al., 1993) and observed in deformation experiments (upscaling: Herwegh & Handy 1996, 1998, downscaling: Tchalenko, 1970). Yet, the length scales
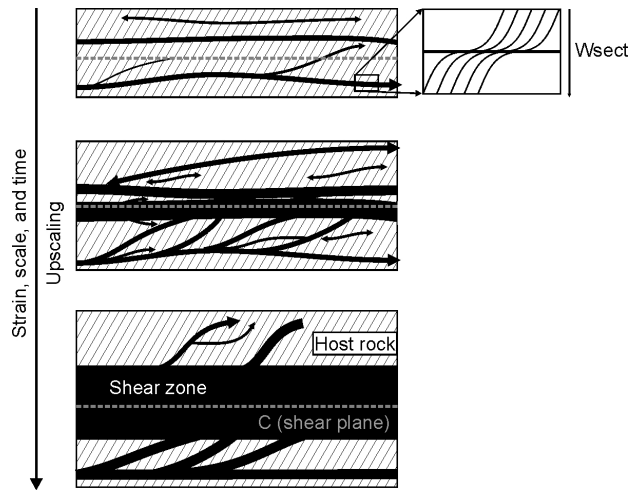
Figure 6.1: Shear zone pattern with strain-dependent change of geometry from isolated shear zones to a shear zone network (center). Line labeled 'C' is the shearing plane. See Fusseis et al., 2006 and Fusseis and Handy, Chapter 5 of this thesis, for models for shear zone networking.

of deformation heterogeneity during these contrasting evolutions have never been quantified.

The need to quantify the scale of deformation arises from the desire to relate scaling characteristics to the micromechanisms of strain localization, as well as to rock physical attributes like anisotropies (foliation, elongate clasts, Dutruge et al. 1995) and rheology (Paterson 2001). Past scaling studies of deformation have invoked fractal statistics to define a range of geometrical scale-invariance (Mandelbrot 1982, Turcotte 1990, Bonnet et al. 2001, Lei et al. 2003) for structures that may be diagnostic of the deformation mechanisms in the rocks analysed. For example, Hippertt (1999) found that the spacing and aspect ratio of S and C shear surfaces in mylonite satisfy a fractal (i.e. power-law) distribution over six orders of magnitude (μm- to km scales). Fractal dimensions have also been used to scale fault systems in the upper, brittle part of the continental crust (Cowie & Scholz 1992a, Bonnet et al. 2001, and references therein). A drawback of this approach is that more than one rock physical attribute can influence the fractal dimension, especially over a broad range of scales. This is especially true of rocks deformed at the transition from pressure-dependent frictional sliding to thermally activated, viscous creep (henceforth termed the brittle-viscous

transition, or BVT), where several competing deformation mechanisms accommodate roughly equal amounts of strain (Handy et al., in press, and references therein). Deviations from a fractal size distribution may also reflect smaller-scale heterogeneities that induce strain incompatibilities and therefore govern rock mechanical behaviour on larger scales (Ackermann et al., 2001). Thus, an analytical scaling method is needed that enables higher spatial resolution and that takes into account the changing physical and kinematic boundary conditions during progressive deformation. In this
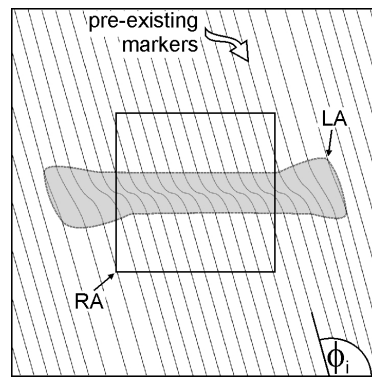
Figure 6.2: Isolated shear zone showing main elements and deformation of ideally passive markers at angle ϕi to the horizontal shearing plane. LA - area of localized deformation (i.e. the shear zone), RA - representative area (see text for explanation).

paper, we introduce a new method for quantifying both the scale and the intensity of strain localization from areal images of natural shear zones. The method employs Autocorrelation Functions (ACF) to determine local scales of geometric homogeneity, so-called elementary reference areas, for calculating scale-dependent localization factors of deformed rock. In a separate step, the intensity of strain localization is quantified relative to an average or background shear strain. We then apply this new method to shear zones from an exposure of the fossil brittle-viscous transition at the Cap de Creus in NE Spain. It is shown that peaks in the scale and intensity of strain localization are related to a combination of existing anisotropies and the networking of brittle-viscous shear zones. We conclude with a conceptual model for the growth and coalescence of shear zones at the BVT involving strain localization on progressively larger scales.

112

6.3 Scaling parameters of shear zones

At least three factors are needed to quantify strain localization on all scales: (1) the proportion of localized deformation per volume of rock on a given scale; (2) the scale-dependence of this proportion; and (3) the degree or intensity of the localization on a given scale. We refer to these three factors, respectively, as the localization factor (LfRA), the scale dependence factor (LfRA as a function of length scale), and localization intensity factor (Iloc). In this section, we introduce these parameters in turn before applying them to determine the scaling properties of some natural shear zones. We note that the approach adopted below can be modified and applied to other structures such as folds. However, this is beyond the scope of our paper.

In the following, we will assume for the sake of simplicity that deformation is isochoric and involves simple shear. Although natural deformation is usually three-dimensional, the deformation in many shear zones analysed so far is nearly plane-strain and highly non-coaxial (Ramsay 1980, White et al. 1980). This is also the case for the shear zones analyzed below, so that all shear zones considered in this paper are regarded at or close to the XZ-plane of the finite strain ellipsoid. Two-dimensional deformation is obviously easier to quantify with our method, but its principles can be extended to three dimensions.

6.3.1 The Strain Localization Factor (LfRA)

Discretely structured matter is usually treated as a continuum by averaging its properties in space based on empirical considerations (e.g. Lai et al., 1993) and determining a homogenization scale (Bonnet et al., 2001). This scale is termed the "representative elementary volume" (REV) and is the smallest relevant volume of the material containing all heterogeneities that appear statistically homogeneous at the scale of observation (Paterson 2001). The averaged mechanical properties of the REV are assumed to control material behaviour at larger scales.

In analogy with the REV for three dimensional strain, we define a "representative reference area", RA, for two-dimensional deformation (Fig. 6.2) in a rock surface that contains undeformed host material as well as all heterogeneities that appear statistically homogeneous on the scale of observation.
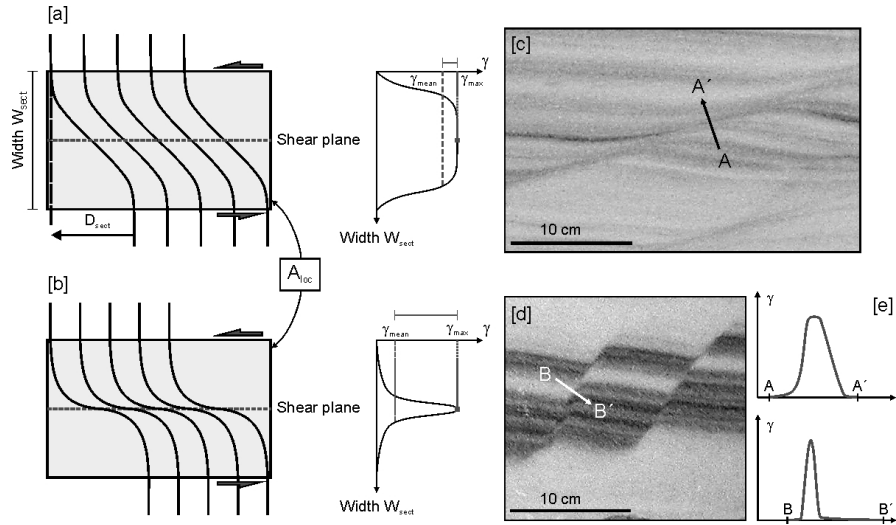
Figure 6.3: Shear strain distributions for two end-member types of shear zones: (a) Displaced markers and shear strain profiles are more homogeneous for the shear zone with low strain intensity (a) than for a shear zone with the high strain intensity (b). The shear zones have the same mean shear strain, γ_{mean}, and displacement, but the maximum shear strains, γ_{max}, differ. Shear zones in marble with low (c) and high (d) strain intensities have different shear strain profiles (e). See text for explanation.

The localization factor LfRA is then defined as a ratio:

$$LfRA = LA/RA \tag{6.1}$$

where LA is the area of a shear zone (Fig. 6.2) within a reference area, RA. LfRA is a dimensionless measure of how much shear zone occurs in a statistically homogeneous area of host rock.

LA is easily determined from a flat image (map or thin section photo) parallel to the XZ plane of a finite strain ellipse with k =1 by measuring the area inside the border of a shear zone. The border is defined by points at which $\delta\gamma/\delta z = 0$, where γ is the shear strain and z the direction perpendicular to the shear plane. Outside of this border, the shear strain is zero or has a constant background value (Ramsay and Graham 1970) because the marker lines at these points do not deviate from their initial orientation, ϕi (Fig. 6.2). In a natural shear zone, the border is defined by an isogon corresponding to zero deviation of a marker, for example, the trace of existing S surfaces.

The determination of RA, is slightly more complicated but crucial. Con-

sider a map of a foliated rock containing a shear zone (Fig. 6.2). Three types of points on the map can be distinguished: (1) points within the shear zone; (2) the shear zone boundary; and (3) points outside the shear zone, within the host rock. On a foliation map these points are distinguished by comparing the orientation of tangents to the marker lines at all points along these lines, ϕP, to a mean orientation of the initial, non-localized marker line, ϕi. A point at $\phi P \in \phi i$ lies outside of the shear zone. Where $\phi P \notin \phi i$, the marker line was rotated beyond the angular interval and is assumed to have been sheared. All points where $\phi P \notin \phi i$ are regarded to lie within the shear zone (Fig. 6.2) and therefore are localized orientations, ϕloc. ϕloc is usually a range of angles because markers in most shear zones are subject to heterogeneous simple shear (Ramsay and Graham 1970).

Obviously, the resolution of shear zone boundaries is best for small variations in the marker orientation outside of the shear zone. In Nature, however, ϕi fluctuates across the outcrop surface due to folding or shearing prior to the activity of the shear zone in question. Therefore, ϕi is given as an angular interval corresponding to the upper and lower limits of all non-localized orientations. If ϕi is highly variable such that locally $\phi loc \in \phi i$, the image must be divided in sub-domains with different local values of ϕi.

Ultimately, we define RA to be the minimum area within which 95% of all marker orientations are undeformed, meaning that a 5% variation in the initial (i.e., undeformed) marker orientation is allowed within RA. The 95% boundary is arbitrary but is a common confidence boundary in statistics (eeg. Bevington and Robinson 1992) and proved to yield good results for the image data below (Fig. 9.8 in Appendix) and in Schrank (2004). Using higher boundary makes our method less robust and results in larger RA, possibly even greater than the map regarded. This must be avoided because an RA larger than the considered map would only satisfy the homogeneity condition if heterogeneities outside the map would be distributed in the same way as in the map. This assumption is unrealistic. The procedure for deriving RA from foliation maps with Autocorrelation Functions is described in Appendices 9.7 and 9.8.

6.3.2 The Strain Intensity Factor (Iloc)

The amount and distribution of strain can vary within a given shear zone area, LA, (Fig. 6.3). In particular, shear strain usually varies both across
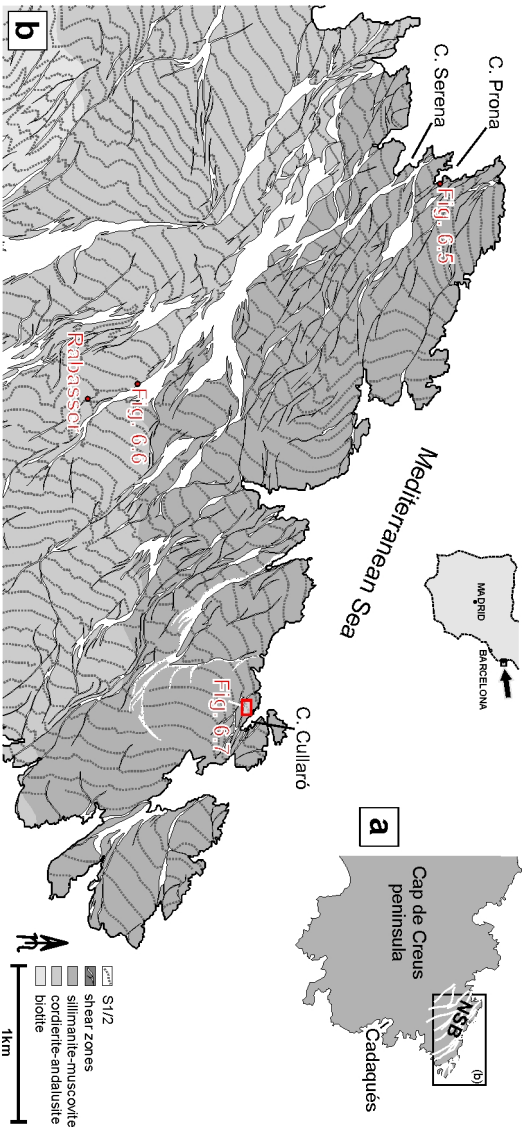
Figure 6.4: Cap de Creus shear zones, after Carreras (2001) and Druguet (2001). (a) Location of the Northern Shear Belt along the northern coastline of the Cap de Creus peninsula; (b) trace of the shear zones (white) and older S1/2 foliation (thin black lines) on the hundred- to thousand-meter scales. Notice locations of Figs. 6.5, 6.6 and 6.7.

116
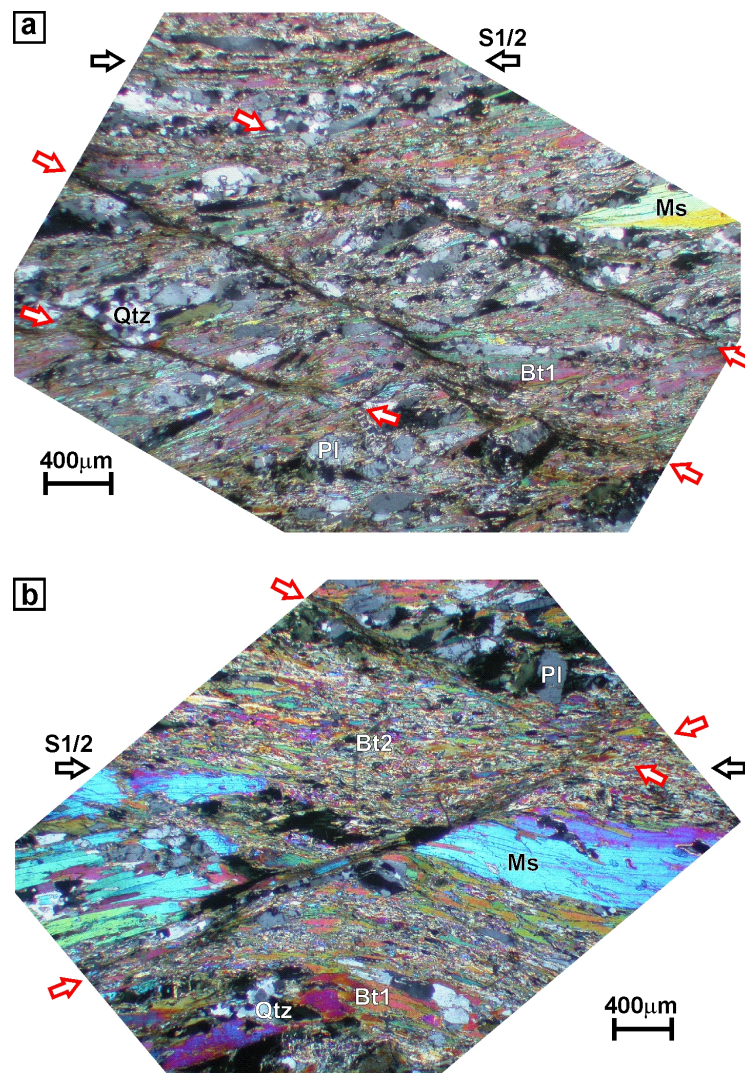
Figure 6.5: Shear zones on the millimeter scale: (a) Preexisting foliation (oriented E/W) defined by biotite-rich domains (Bt) alternating with microlithons of elongate quartz (Qtz) and minor plagioclase (Plag), displaced by millimeter-ling shear bands. Ms - muscovite porphyroclasts. In both S1/2 and the shear bands, Bt reacted syntectonically to form fine-grained aggregates of secondary Bt2, Ms, chlorite (Chl) and ilmenite (Ilm). (b) Boudinaged Ms porphyroclast, preexisting foliation oriented E/W. Note fine-grained aggregates of Bt2, Ms, Chl and Ilm. See text for explanation. Both pictures are taken from thin sections oriented parallel to the XZ plane with cross-polarizers. Sample CC08, location in Fig. 6.4b, composition in App. 9.3.

and along shear zones (eeg. Ramsay & Graham, 1970), and this variation becomes more pronounced with increasing finite shear strain (Fusseis et al.,

2006). We define strain intensity to be the amplification of shear strain above an average value of shear strain in the same shear zone. Strain intensity is illustrated in Figure 6.3 by profiles of shear strain versus distance across the centres of two hypothetical shear zones. The shear zone with a homogeneous strain distribution has a broad profile with a flat top (Fig. 6.3a), whereas the shear zone with a heterogeneous strain distribution has a profile with a high narrow peak above a wide, low base (Fig. 6.3b). The latter profile indicates a greater strain intensity because higher shear strains are concentrated in a narrower zone, i.e., the strain is distributed more heterogeneously. Thus, the shape of the shear strain profile is diagnostic of the variability and intensity of strain within a shear zone (Ramsay & Graham, 1970).

Natural shear zones often have irregular, asymmetric shear strain profiles (Fig. 16 in Ramsay & Graham, 1970, Simpson, 1983, Hull, 1988, Lamouroux et al., 1994) that require complicated mathematical descriptions to quantify strain localization. To avoid these complications, we propose using a combination of the easily obtainable, geologically relevant parameters, γ_{mean} and γ_{max}, to describe the intensity of strain localization across shear zones. γ_{mean} is the average shear strain of the shear zone, whereas γ_{max} is the maximum shear strain within the shear zone (Fig. 3). γ_{max} can be calculated from the angles of deflected and undeflected markers by the relationship (Ramsay & Graham, 1970):

$$\gamma_{max} = \cot \alpha - \cot \alpha' \tag{6.2}$$

where α is the initial angle (i.e. undeformed orientation) of a marker line and α' is the angle of maximum deflection within the shear zone, both measured with respect to the shear plane. γ_{mean} can be obtained from the relation:

$$\gamma_{mean} = D_{sect}/W_{sect} \tag{6.3}$$

where D_{sect} is the total displacement along a shear zone of width W_{sect} measured at the same location as the strain profile above. If strain markers are available, the displacement can be measured directly. Otherwise, it may be determined from the area under the strain profile curve according to the relation (Ramsay & Graham, 1970):

$$D_{sect} = \int_0^{W_{sect}} \gamma \, dz \tag{6.4}$$

118

For homogeneous profiles, γ_{mean} is close to γ_{max}. The difference of γ_{mean} and γ_{max} is small (Fig. 3a). For heterogeneous strain profiles, γ_{mean} is small due to the high proportion of small shear strain values. The difference of γ_{mean} and γ_{max} is large (Fig. 6.3b). The difference of γ_{mean} and γ_{max} normalized to γ_{max} is used as a measure of strain intensity, Iloc:

$$Iloc = \frac{\gamma_{max} - \gamma_{mean}}{\gamma_{max}} = 1 - \frac{\gamma_{mean}}{\gamma_{max}} \tag{6.5}$$

For shear zones with homogeneous strain profiles and low strain intensity, the ratio of γ_{mean} to γ_{max} becomes large and Iloc tends to zero. Shear zones with heterogeneous profiles and high strain intensity have small ratios of γ_{mean} to γ_{max}, so Iloc tends to one. Natural examples of shear zones with low and high strain intensities are shown in Figures 6.3c and d.
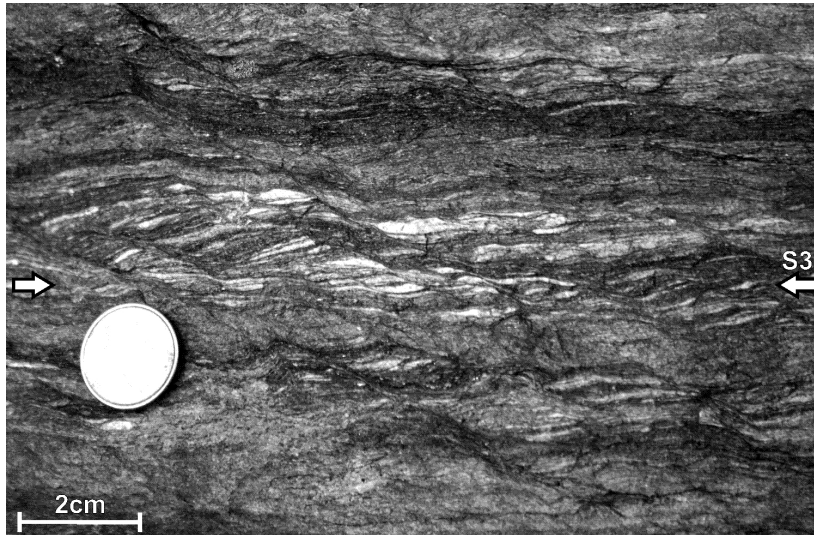
Figure 6.6: Shear zone on the centimeter to decimeter scales. Outcrop location marked 'Fig. 6.6' in Fig. 6.4b. See text for explanation.

6.4 Application of Scaling Methods to the Cap de Creus shear zones, NE Spain

6.4.1 Geology of the shear zones

Shear zones within the Northern Shear Belt at the Cap de Creus peninsula of NE Spain (Fig. 4) are ideally suited for testing the scaling methods de-

veloped above. This shear belt is a deeply eroded part of a fossil, plate-scale fault that accommodated dextral transpressional motion in Early Permian time (Carreras 2001). The shear belt evolved during a continuous, retrograde deformational event that initiated at upper amphibolite-facies conditions (Carreras & Druguet, 1994, Druguet et al., 1997, Alfonso et al., 2003, Bons et al., 2004) and that ended under retrograde greenschist-facies conditions at 350-450°C and 0.3 GPa (Carreras, 2001, Druguet, 2001, Fusseis et al., 2006). The greenschist-facies shear zones analyzed below affected metasediments that contain an earlier composite foliation (S1/2). This foliation is orientated regionally at high angles (70-90°) to the mylonitic shearing plane (Fig. 6.4b, Carreras, 2001, Fusseis et al., 2006), but adjacent to the shear zones is deflected towards this shearing plane. S1/2 therefore served as an excellent marker for the quantification of displacement and strain (Fusseis et al. 2006). Pegmatites and granitoids concordant to S1/2 are cut by and therefore predate the greenschist-facies shear zones. These magmatic rocks are inferred to have intruded synkinematically during the peak stages of upper amphibolite-facies deformation (Carreras & Druguet, 1994, Druguet et al., 1997, Alfonso et al., 2003, Bons et al., 2004).

To interpret the scaling characteristics of the shear zones below, it is crucial to understand the evolution of these shear zones as inferred from a spatial sequence of strain and structures in outcrop (Fusseis et al., 2006): The shear zones nucleated as shear fractures parallel to the later mylonitic shearing plane. Increasing displacement on these fractures lead to the development of a mylonitic foliation along the central segments of the fractures while their brittle tips continued to propagate. In this way, the shear zones lengthened and eventually interconnected to form a network of mylonitic shear zones. Thus, networking represents a strain-dependent switch from brittle to viscous deformation on the scale of the shear zone network. The network comprises host shear zones oriented parallel to the shearing plane linked by step-over shear zones that propagated parallel or at low angles to S1/2, but at high angles to the host shear zones. This network isolates lozenges of less-deformed country rock, that were progressively overprinted as the shear zones broadened. Deformation therefore homogenized on a larger scale than at the onset of strain localization.

Slip-line analysis of the mylonitic foliations and stretching lineations in the shear zone network reveals that deformation was dominantly simple

shear on the scale of the network (Fusseis et al. 2006). On the millimeter-
to decameter scales, the shear zone margins are marked by deflected S1/2
foliation trajectories adjacent to the shear zone centers containing a pene-
trative C foliation (Fusseis & Handy, Chapter 4 of this thesis). On all larger
scales, the margins are relatively narrow compared to the centers. The coun-
try rock is itself heterogeneous, with alternating micaceous and quartz-rich
sequences up to tens of meters thick. These features are shown below to
affect the scaling of the shear zones.

6.4.2   Determination of LfRA for different scales

LfRA was determined for shear zones mapped onto photographs of thin
sections and outcrops, aerial photographs and as well as shown on structural
maps of the Cap de Creus peninsula (Figs. 6.5 to 6.7), and then plotted
against the log of shear zone length (Fig. 6.8) and maximum shear zone
width (Fig. 6.9). Data used in these figures is listed in Table 6.1. The
names and localities of the samples analyzed below are shown in Figure
6.4b.

The data clusters in Figure 6.8 can be fit to a power law function:

$$LfRA = A \cdot l^d \qquad (6.6)$$

where A and d are power law parameters for each scale, and l is the shear
zone length. A similar, though poorer fit with the same parameters was
obtained for a plot of LfRA versus shear zone width (Fig. 6.9). The geo-
metric and mechanistic significance of these parameters is discussed in the
next section. The analysis of two-dimensional images is beset with two basic
problems: First, because shear zone geometry varies in the Y direction, i.e.,
parallel to shear zone foliation (XZ plane) and perpendicular to the transport
(X) direction, their lengths and widths are systematically underestimated.
This "truncation effect" is especially pronounced for small shear zones (Bon-
net et al. 2001), but is probably minor for the Cap de Creus shear zones
in light of evidence cited above for simple shearing. Second, shear zones on
the kilometer-scale are often longer than the largest areas imaged. Indeed,
the largest shear zones at the scale of the Pyrenean mountain belt cannot
be analyzed due to our basic inability to see them in their entirety at the
surface. This selectivity or "censoring effect" leads to a bias towards the
analysis of small-scale structures. Both the truncation and censoring effects
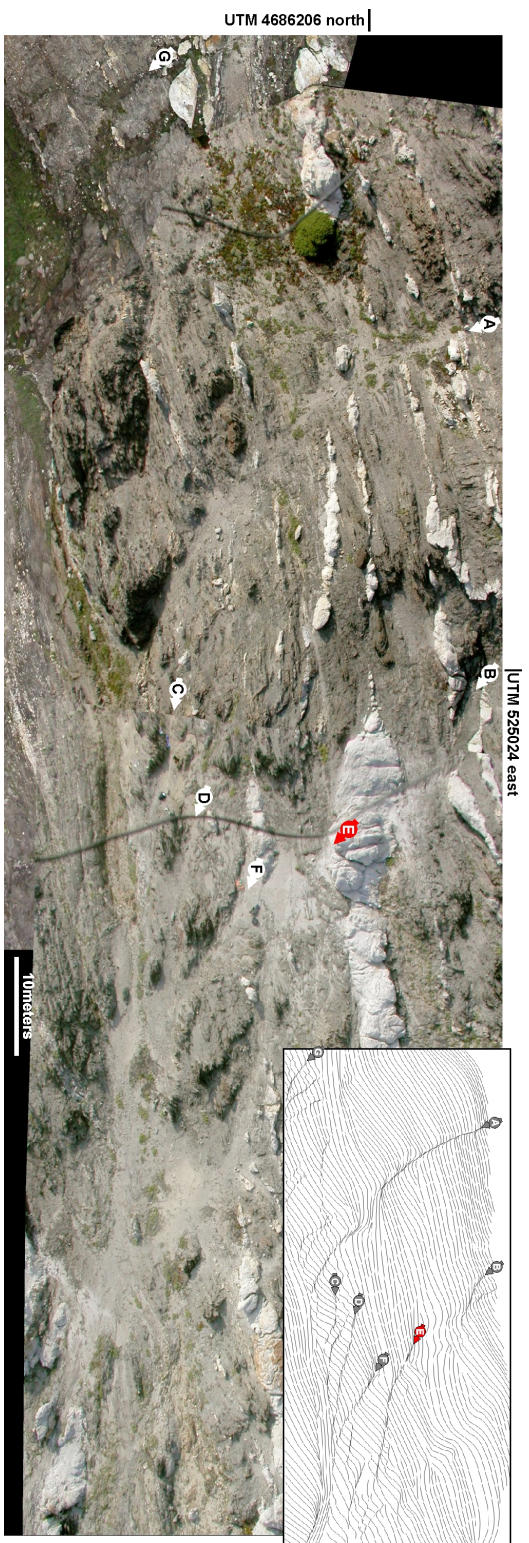
Figure 6.7: Shear zones on the scale of tens of meters. Kite aerial photographs merged by R. Christmann. See Fig. 6.4b for location and text for explanation.

122

| Locality	Fig. in text	UTM	Lf_{RA} maximum (%)	D_l	A_l	Dw	a_{RAc}	a_{RA}	Type of anisotropy	Width interval of anisotropy
Cala Prona (thin section)	6.5	521770 east 4687428 north	1,4	1,04	$12.81*10^{-3}$	1,64	8.5 mm	1.5 cm	Spacing of cleavage domains Ms clasts	[1;5] mm [0.5;2] mm
Rabasser Metapelites	6.6	523135 east 4685456 north	18,0	1,40	$14.32*10^{-3}$	0,66	1.8 cm	3.2 cm	Spacing of cleavage domains	[0.04;2.4] cm
Rabasser Quartzites	not shown	523151 east 4685181 north	16,1	1,48	$11.88*10^{-3}$	1,52	4.0 cm	7.0 cm	Spacing of cleavage domains	[0.03;2.2] cm
Cala Cullaro	6.7	525024 east 4686206 north	18,4	1,42	$13.18*10^{-7}$	0,73	13.5 m	23.9 m	Pegmatite thickness	[0.01;8.4] m
Northern Shear Belt	6.4b		4,2	1,71	$4.43*10^{-12}$	1,71	2369 m	4199 m	Metamorphic gradient?	?

Table 6.1: Locations and quantitative analysis of investigated shear zones at the Cap de Creus. See text for explanation.

123

are unavoidable in any imaging method (Bonnet et al. 2001) and are reflected in the considerable scatter of the data; the power law fit to the data in Figure 6.8 has squared correlation coefficients, r^2, of between 0.80 and 0.94. The r^2-value of the Rabasser metapelites for the data on shear zone width (Fig. 6.9) is even lower (0.19). This scatter must be kept in mind when interpreting the results below. Fortunately, we can rule out sampling bias (e.g. Nicol et al 1996) as an explanation for the scale dependent effects on rock structure, because the excellent outcrop exposure at Cap de Creus preclude any observational gaps; we actually see localization structures and existing anisotropies from the grain-scale to the scale of the entire peninsula.

Figures 6.8 and 6.9 reveal some interesting trends (cf. Table 6.1). First, there is a striking gap in the scale of localization over lengths of several decimeters to meters, and widths of centimeters to decimeters. This contrasts with overlaps of both localization length and width at other scales. Second, the scales of pre-existing anisotropies (foliation spacing, sedimentary layer thickness, pegmatite width) coincide with the characteristic length scales of RA. Third, the exponential length-scaling factor, Dl, is nearly 1 for the smallest shear zones on the millimeter- to centimeter-scales and increases with length scale, attaining a value of 1.71 for 100m- to km-long, crustal-scale shear zones (Fig. 6.8). Only the shear zones on the 10m scale (Cala Cullaro data in Fig. 6.8) deviate slightly from this trend. The width-scaling exponent, Dw, also varies with shear zone width but less systematically. The correlation coefficients for the power-law fits are poor due to increasing importance of measurement errors (the width determination error is larger compared to shear zone width than to shear zone length) and other reasons. In the following, we describe possible causes for these trends, especially the effects of existing structure and deformation mechanisms that operate on different scales.

6.5   Interpretation and discussion

Several factors affect the geometry of shear zones, foremost the lithology and inherited structure (i.e., the structure existing prior to the formation of the shear zones) as well as the deformation mechanisms and rheology of the rocks during shearing. These are considered below, with reference to the
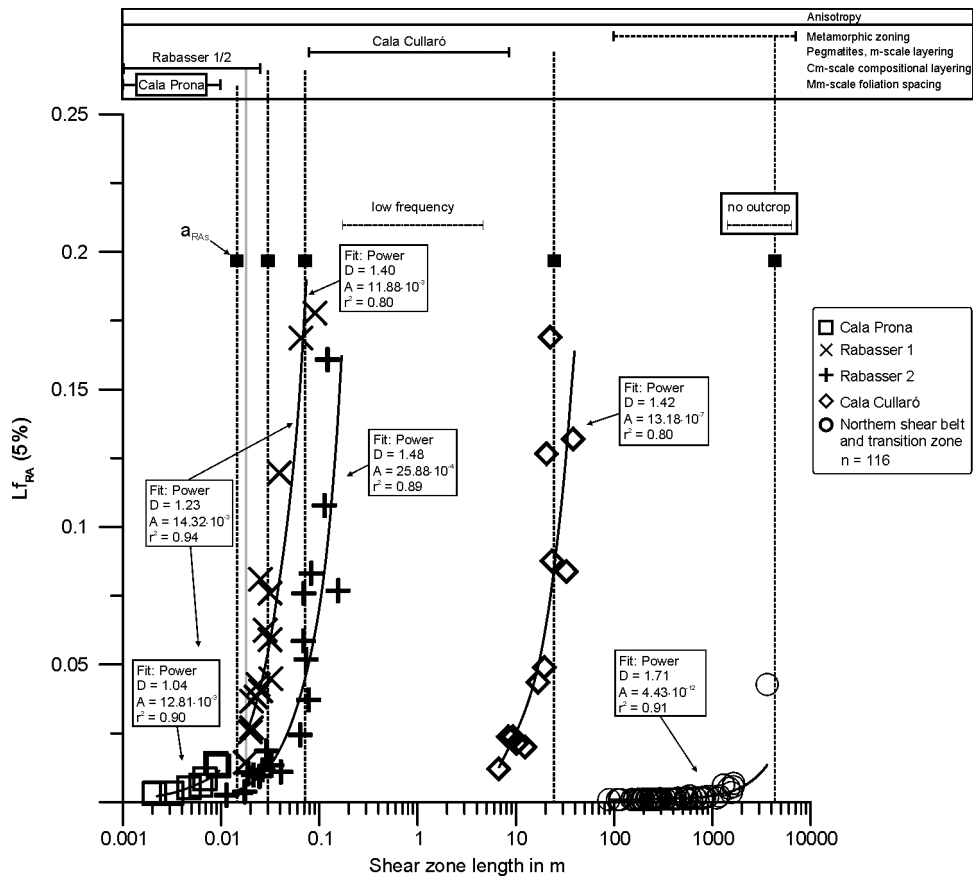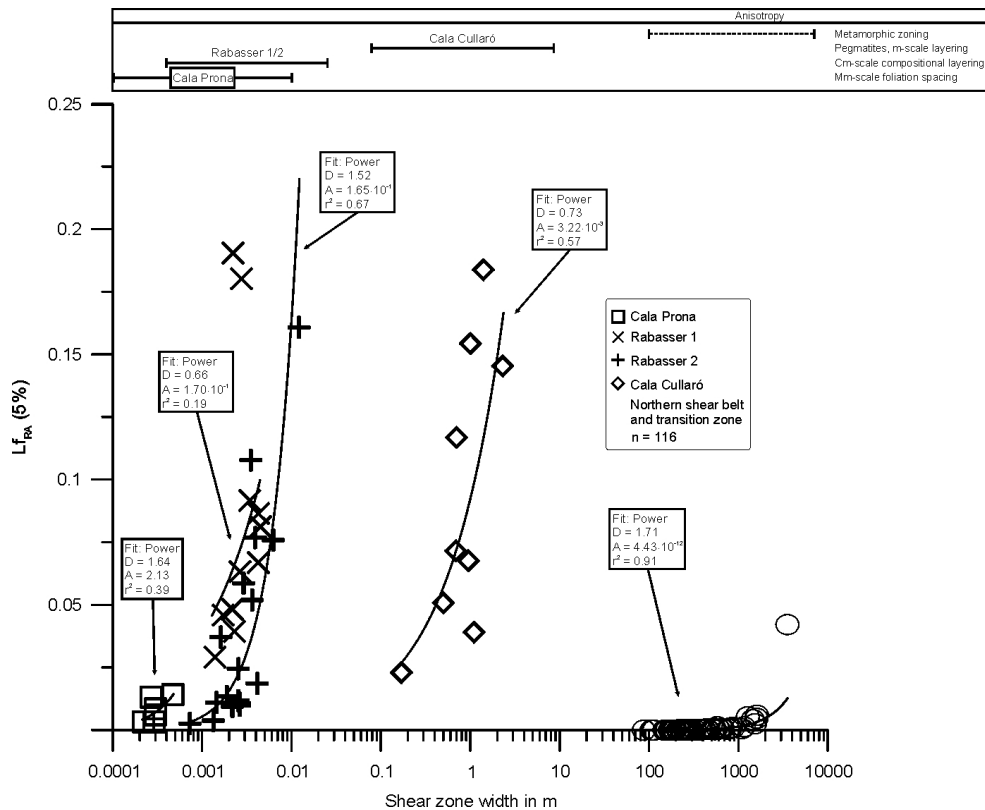
Figure 6.8: Localization factor (LfRA) versus length of the shear zones in the Cap de Creus area. Description of measurement technique given in text. Box above the plot shows the range of lengths of existing (inherited) anisotropies as measured in thin section and outcrop. The bar for the largest-scale data labeled "metamorphic zoning" is estimated from maps of Carreras (2001) and Druguet (2001), as depicted in Fig. 6.4b.

structures shown in Figures 6.4 to 6.7 and the aforementioned trends in the scaling properties in Figures 6.8 and 6.9 and Table 6.1.

6.5.1 The role of mechanical anisotropies

The length- and width-scales for some of the Cap de Creus shear zones correlate quite well with the range of widths of pre-existing anisotropies, whereas the correlation is poor with the lengths of these same anisotropies, as plotted on identical horizontal logarithmic scales at the tops of Figures 6.8 and 6.9. This close relationship between the scale of localization and the width

Figure 6.9: Localization factor (LfRA) versus maximum width of the shear zones in the Cap de Creus area. Box above the plot shows the range of widths of existing (inherited) anisotropies as measured in thin section and outcrop. The bar for the largest-scale data labeled "metamorphic zoning" is estimated from maps of Carreras (2001) and Druguet (2001), as depicted in Fig. 6.4b.

of inherited structures can be seen in the rocks themselves. On the smallest (millimeter-) scale, the shear bands emanate from micaceous domains in S1/2 and from the edges of muscovite clasts (Fig. 6.5a), whereas on the centimeter-scale (Fig. 6.6) the shear bands are developed in alternating, foliated layers of micaceous schist ($\sim$ 0.05 to 2.5cm wide) and boudinaged quartz aggregates. The meter- to decameter-long shear zones (Fig. 6.7) also splay from such layers, as well as from the margins of decimeter- to 10m-wide pegmatite bodies (see red arrow in Fig. 6.7, Druguet et al., 1997). No inherited anisotropies are evident on scale of the kilometer-scale shear zones, possibly explaining the lack of a peak in the LfRA values for this scale. However, it is notable that these large shear zones are restricted to

126

the part of the Northern Shear Belt with the highest metamorphic grades (cordierite - andalusite /sillimanite - muscovite; Druguet 2001) and are oriented subparallel to the metamorphic isograds (Fig. 6.4).

These relationships suggest that the mechanical and geometric properties of existing anisotropies control localization on the same or similar scales. On the millimeter scale, nucleation of shear bands along muscovite clasts and micaceous layers may reflect stress concentrations that arise from strain incompatibilities between the micas and the adjacent quartz-rich layers undergoing predominantly dislocation creep (Fusseis and Handy, see Chapter 4 of this thesis). Such stress concentrations can either locally enhance creep (Lloyd & Knipe 1992, Mainprice et al. 2004) or induce shear fracturing (Gottschalk 1990, Shea & Kronenberg 1993), especially in the presence of a fluid at hydrostatic to near-lithostatic pressure (Bauer et al. 2000a, b). Indeed, Shea & Kronenberg (1993) found that shear fractures nucleated in microlithons in experimentally deformed mica schist; they emphasized the importance of the initial spacing and concentration of micas and non-micaceous aggregates in nucleating such fractures. The shear bands in Figure 6.5 are interpreted to have formed as transgranular shear fractures during the early stages of strain localization, then to have undergone a combination of diffusion-accommodated grain-boundary sliding in quartz and plagioclase, and basal [001]-glide in newly crystallized micas (Fusseis and Handy, see Chapter 4 of this thesis).

Lithological control of localization is also evident at the margins of centimeter- and decimeter-scale shear zones, where quartz-rich layers subparallel to S1/2 are smoothly deflected across the shear zone (i.e, show moderate values of Iloc), whereas micaceous layers are bent sharply (highly localized strain, high Iloc values) and completely thinned out in the mylonitic centres of the shear zones. This corroborates many experimental and theoretical studies showing that strain localization is governed by the mechanical properties (e.g. viscosity contrast, number and thickness of layers, Ramberg 1955, Biot 1964) as well as the orientation of existing anisotropies (e.g. schistosity, sedimentary layering) with respect to the shearing plane (Cobbold et al. 1971, Cosgrove 1989, Williams & Price, 1990).

The general coincidence of kilometer-scale shear zones with the orientation and location of regional metamorphic zones (Fig. 6.8) may be fortuitous, but may also reflect the inherited effects of earlier metamorphism
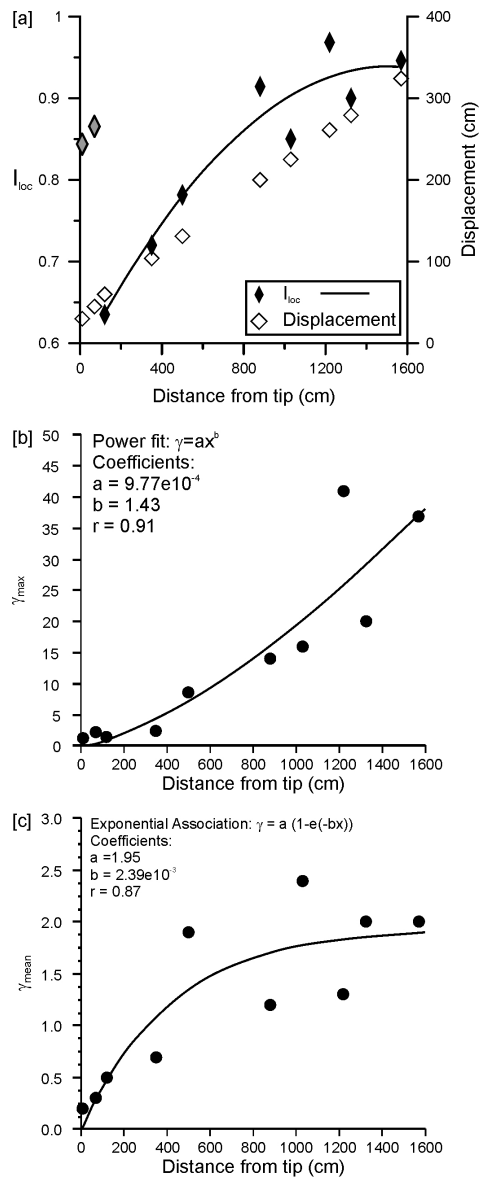
Figure 6.10: Plots of various measures of localization versus distance from the tip to the centre of a single, m-scale shear zone in the Cap de Creus area: (a) Localization intensity, Iloc, and displacement; (b) maximum shear strain; (c) mean shear strain. Distance on the horizontal axis is used as a proxy for time during shear zone evolution, increasing to the right (see text). Black lines show best-fit functions to the data (discussed in text).

and magmatism on rock rheology during shearing. Specifically, prograde metamorphism culminating in the intrusion of pegmatitic dykes prior to the formation of the shear zones (e.g. Druguet & Hutton 1998, Alfonso et al.

2003) may have lead to spatial variations in the rocks' volatile content, especially in their water concentration. Rock deformation experiments have documented the weakening effect of volatiles, especially of water, on silicate mineral aggregates undergoing inter- and intragranular creep (e.g. review in Carter & Tsenn 1987). Given the ubiquity of microstructures that are diagnostic of dislocation creep in the largest shear zones at Cap de Creus (Fusseis et al. 2006), it is tempting to speculate that these shear zones nucleated and grew preferentially in areas that had previously been enriched in fluids during prograde devolatilization reactions and magmatism.

Interestingly, the width of a square representation of RA, a_{RAs}, coincides with the maximum scale of the underlying anisotropies with an accuracy better than an order of magnitude. Since RA has been arbitrarily defined to contain 5% localized areas by the means of the ACF, this relation might be accidental and requires further testing with other data. Nevertheless, given the assumption that localization depends on pre-existing heterogeneities within characteristic scales, one would intuitively expect a correspondence between a reasonable statistical homogenization scale and the length scale of mechanical anisotropies. If this correspondence is no artefact, we observe that the homogenization scale (and with it, the scaling or growth law) jumps to the next scale, once the largest shear zones attained a length close to the width of RA. This behavior would be consistent with the notion that the effective mechanical layer thickness of the localizing rock volume affects the scaling behavior (Ackermann et al. 2001). It seems intuitively reasonable that the scaling behavior of the shear zones changes as soon as the longest shear zone crosscuts the entire geometrical homogenization area (or volume in 3D), considering that the averaged properties of the homogenization scale govern localization at that given scale.

We conclude this section with the observation that peaks in the localization factor do not always correspond with the scales of existing anisotropies. For example, shear zones that are tens of meters long (Cala Cullaro, Fig. 6.7) are longer than the width of the largest pegmatitic bodies. This mainly affects the LfRA-length data (Fig. Figs. 6.8). Possible reasons for that are: a) data censoring effects leading to peak underestimation. b) Shear zone length scaling is probably controlled by the effective mechanical layer thickness of the host rock (Ackermann et al. 2001). Since the regarded shear zones typically are oriented at angles smaller than 90° with respect

129

to the anisotropies, they can grow longer than the mechanically relevant maximum layer width before they cross-cut these layers and the scale jump occurs. c) Other factors alter scaling behavior. In the next section, we therefore explore the idea that strain and the active deformation mechanisms, in addition to existing anisotropies, are important determinants of the scales of localization.

### 6.5.2 The effects of strain and kinematics

It was noted above that Dl varies with increasing length scale from about 1 (quasi-linear) to 1.71 (nearly quadratic, Fig. 6.8)[2]. The relative values of Dl and Dw (Table 6.1) suggest that the aspect ratio of the shear zones first increases with scale and ultimately decreases at the largest scale. In other words, small shear zones are comparatively slender, whereas big ones tend to be broader with respect to their length. This is easily confirmed by comparing the geometries of shear zones on different scales (cf. Figs. 6.4b, 6.5). The slight deviation of the Dl value for the shear zones at the Rabasser 2 locality ('Rabasser' in Fig. 6.4b) from this general trend may reflect the different rheology of the quartz-rich rocks at this locality than for the miceaceous rocks hosting the shear zones in the other localities.

The decrease in the aspect ratio of shear zones with increasing scale manifested in the D values belies strain-dependent changes in the dominant deformation mechanisms from brittle deformation (fracturing, cataclasis) to viscous, mylonitic shearing. These changes are in turn closely tied to a structural transition from isolated to networked shear zones, as described by Fusseis et al. (2006).

At low shear strains on the grain scale, localization involves fracturing antecedent to viscous creep, as described above. This is reflected by the nearly linear scaling relationship for the shear bands at Cala Prona in Figure 6.8, which originated as shear fractures and are thin, planar features (Fig.

---

[2]Dw is more difficult to interpret for the following reasons (Figs. 6.9). First, the relevance of measurement errors becomes more important and increases data scatter. Second, the width variation of the two smallest-scale data sets (Cala Prona and Rabasser 1) covers less than half an order of magnitude in contrast to all other data sets. This decreases the goodness of the power-law fit (compare correlation coefficients in Fig. 6.9, Bonnet et al. 2001). It also implies that the width of shear zones at these scales remains nearly constant during growth. Hence, power-law distributions are inherently not suitable for approximating these data.
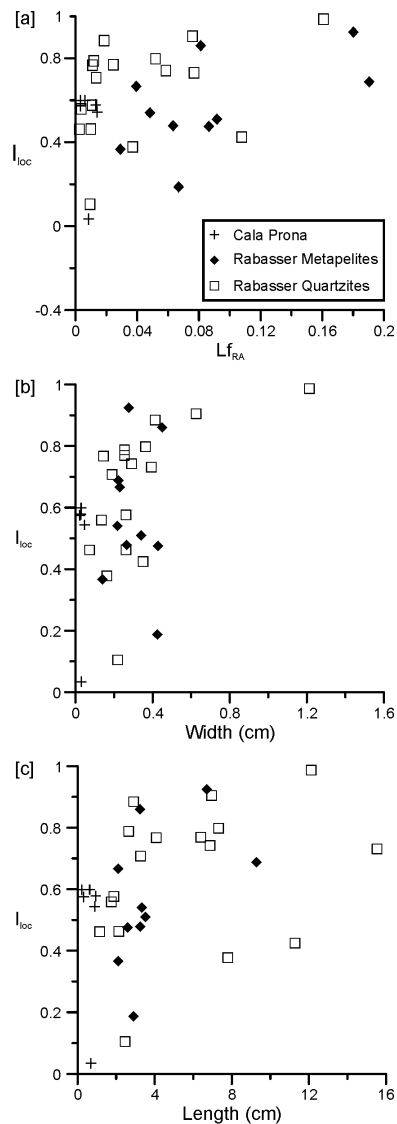
Figure 6.11: Plots of strain intensity factor, Iloc vs. the localization factor, LfRA (a), the log of shear zone lengths (b) and widths (c) for all available shear zones on the scales considered in this study (symbols for shear zones from different localities given in box).

6.5a). They accommodated extension parallel to the shearing plane and subparallel to the dominant S1/2 foliation, as shown by the conjugate shear bands in Figure 6.5b. At centimeter- to decimeter length scales (Rabasser data, Fig. 6.8), the attainment of a nonlinear Dl value is associated with the dominance of viscous creep mechanisms in the center of the shear zones (dislocation creep in quartz, glide parallel to the basal [001]-crystallographic

plane in micas, diffusion-assisted grain-boundary sliding in fine-grained qtz-fsp-mica aggregates, Fusseis and Handy, Chapter 4 of this thesis). Quartz-rich layers are asymmetrically boudinaged and have rotated between mica-rich layers (Fig. 6.6). These boudins are interpreted as "shear band boudins" (Goscombe et al. 2004) that formed during multilayer extension parallel to S1/2 (Gosh and Sengupta 1999).

For shear zones at length scales of meters- to tens of meters, Dl becomes only slightly more nonlinear (Cala Cullaró data, Fig. 6.8) than for centimeter- to decimeter scale shear zones. Up to this crucial range of length scales, fracturing is inferred to have been active during mylonitic shearing; the fractures formed at the tips of longitudinally propagating mylonitic shear zones that are just locally interconnected (Fusseis et al. 2006). Although some of these shear zones evidently nucleated on the same length scale as existing anisotropies (described above), many of them are clearly longer than the width of these anisotropies (Fig. 6.8) as they have grown longitudinally in a direction subparallel to the shearing plane. This growth explains the gap in localization data at the 10m length scale in Figure 6.8. Our field measurements indicate that the deformation within these shear zones changes from brittle to mylonitic where displacement exceeds a critical value of about 1-2 m (Fusseis et al. 2006). As shown in the next section, the mylonitic centers of these shear zones experienced softening, thus facilitating the lateral propagation of these shear zones.

The dramatic increase in Dl to nearly 2 for shear zones at length scales of hundreds to thousands of meters (Fig. 6.8) is clearly related to the establishment of a network of anastomosing mylonitic shear zones (Fig. 4b). At this scale, fracturing is subordinate to mylonitic deformation, such that the networking of smaller scale shear zones can be interpreted to coincide with a transition from brittle to viscous deformation at the crustal scale (Fusseis et al. 2006). The shear zones depicted in Figure 6.7 are C´ surfaces with respect to the regional shearing plane, represented by the mylonitic foliation at the bottom of the figure. These anastomosing shear zones broaden with increasing strain, eventually incorporating meter- to 10m size blocks or lozenges of less-deformed rock (Fusseis et al., 2006). This lateral homogenization process is reflected in the maximum Dl value of 1.71 at the largest scale. The lozenges are inferred to have rotated during deformation, a process which previous studies have shown can accommodate greater

strains without lengthening the host faults (Gross et al. 1997). Therefore, both broadening of the networked shear zones and block rotation of lozenges within this network may be responsible for the reduced aspect ratio of the 100m to km-scale shear zones as inferred from the relative Dl and Dw values cited above.

The change of the localization exponent, Dl, with increasing length scale primarily reflects a progressive increase in the scale of localization, a process which we termed "upscaling" in the introduction (Handy et al., in press). Upscaling can also be regarded as a delocalization (or increasing homogenization) of strain on any given scale, and is governed by the strain-dependent transition from brittle to viscous deformation on progressively longer length scales. The change in Dl values with shear zone length can therefore be regarded as an empirical growth law for mylonitic shear zones.
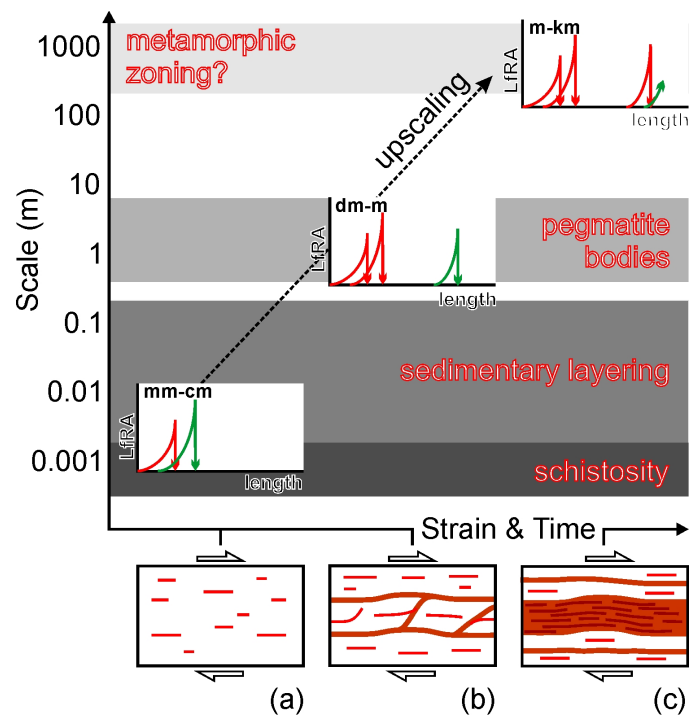
Figure 6.12: Conceptual model for the evolution of shear zone scale with bulk strain. (a) Initial fracture nucleation and propagation; (b) attainment of critical displacement and lengths of fractures for networking; (c) lengthening and broadening of the shear zone network on the km scale. The scale of localization increases as the shear zones propagate and link up to form interconnected weak layers parallel to the shearing plane (see text). Gray bars indicate range of scales of inherited mechanical anisotropies.

133

6.5.3   Do shear zones soften or harden during upscaling?

It is generally accepted that brittle and mylonitic rocks have different rheologies (e.g. Handy, 1989), but how does rheology change during upscaling? Insight into this question comes from the distribution of the strain intensity factor, Iloc, along and across the center of both individual and networked shear zones. Recall that Iloc is a measure of the heterogeneity (i.e., the shape) of a shear strain profile across a shear zone (Fig. 6.3). Previous workers suggested that the temporal evolution of such profiles yields insight on the changing rheology of the deformed rocks (Hull, 1988, Lamouroux et al., 1994, Means, 1995).

Inspired by Means (1984), Hull (1988) distinguished three end-member types of shear zones. Type I zones harden with time. They broaden during growth and exhibit flat-topped, homogeneous strain profiles such as that shown in Fig. 6.3a (see Fig. 4 in Hull 1988). Iloc is small and, in an actively hardening and broadening Type I shear zone, would continuously decrease after an initial stage of growth related to pre-localization elastic loading and shear zone nucleation. Type II shear zones soften in their centers and are expected to narrow with time. The resulting shear strain profile would become increasingly heterogeneous over time with a narrowing, growing central peak. Iloc would have rather high values and increase as long as the center of the shear zone weakens with respect to its margins. Type III shear zones remain at steady state. They maintain a homogeneous strain distribution (e.g. homogeneous simple shear). This behavior is exemplified by kink bands; Iloc would remain at a constantly low value during kinking. Obviously, these end-member types of shear zones only bracket the range of possible shear zones evolutions in Nature; they are conceptual vehicles for interpreting real strain profiles.

Provided that spatial variations in strain are a valid proxy for time (Mitra, 1984, Means, 1995, Fusseis et al., 2006, Holyoke & Tullis, 2006), we can use variations of Iloc across and along shear zones to reconstruct temporal and spatial variations in relative strength during shearing. To this end, we plotted several shear strain parameters versus the distance from the tips to the centres of a single mylonitic shear zone (Fig. 6.10) on the premise that the displacement gradient over this distance (Fig. 6.10a) reflects a time sequence of the shear zone evolution. That is, progressively older fabrics are preserved from the tip to the centre of the shear zone.

The assumption that spatial variations in structure and shear strain reflect temporal variations in the Cap de Creus shear zones is justified by structural and metamorphic evidence that shearing on the crustal scale occurred during one continuous, kinematically simple event (simple shearing) under retrograde greenschist-facies conditions (Druguet 2001, Fusseis et al. 2006). We note that the calculated values of the strain intensity factor, Iloc, in Figures 6.10 and 6.11 are subject to uncertainties in the determination of maximum shear strain (see Appendix 9.2 for a detailed discussion). Although such estimates are fairly reliable for shear zones on length scales up to 10m, it is unfortunate that no markers for determining shear strain are available for the Northern Shear Belt as a whole.

Displacement along a single shear zone at Cala Prona (location in Fig. 6.4b, same as for Fig. 6.5) increases steadily from the tip to the centre of the shear zone, indicating that deformation was probably continuous on the time scale of shear zone activity (Fusseis et al. 2006). Iloc increases with this distance as well and is best fit by a quadratic polynomial function (black line). The two displacement data points close to the shear zone tip (light-grey diamonds) are not used in this analysis because they involve decimeter-long shear fractures in the tip damage zone that yield intrinsically high Iloc-values and are therefore not comparable to the mylonitic parts of the shear zone discussed here.

We interpret the increase in Iloc values from tip to centre to reflect strain weakening of the shear zone centre relative to the tips. As pointed out before (Fusseis et al. 2006), weakening can also be inferred from the evolution of maximum shear strain (γ_{max}) and mean shear strain (γ_{mean}) depicted in Figures 6.10b and c. The γ_{max}- and γ_{mean} data are best fit by power-law and exponential functions, respectively (black lines in Figs. 6.10b, c). Because both plots refer to identical distance intervals (and hence time steps) in the same shear zone, the nonlinear best-fit curves indicate that the strain rate in the shear zone centre accelerated with respect to the strain rate at the shear zone tips.

To investigate how weakening scales with shear zone size, we plotted Iloc versus the localization factor, LfRA (Fig. 6.11a), shear zone length (Fig. 6.11b), and shear zone width (Fig. 6.11c) for all available shear zones at the Cap de Creus. The Iloc values are calculated from shear profiles where maximum displacement occurred. The smallest-scale shear zones

(Cala Prona locality, Figs. 6.4b, 6.5) have moderate to high intensity factors and low localization factors (Fig. 6.11a), and their intensity factors are effectively invariant with length and width (Figs. 6.11b, c). In other words, the strain does not intensify significantly during shear band growth. Their width varies little with their length (Fig. 6.5) so that the strain distribution within these shear bands is rather homogeneous when regarded at the scale of a thin section. For the cm-scale shear zones (Rabasser 1 and 2), Iloc correlates positively with both length and width (Figs. 6.11b, c), suggesting that strain intensifies during growth of the shear bands. We interpret this to indicate strain weakening within the shear bands, probably due to the increasing activity of dynamic recrystallization.

The scatter of the Rabasser data in Figure 6.11a indicates that factors other than strain (e.g. location of the samples adjacent to foliation lozenges or competent bodies like pegmatites) may influence strain intensity and localization factors at this scale. Larger scale shear zones (meter- to 10m scales) show a greater scatter of data points and only ill-defined trends, if any; strain intensity factors cover a broad range of localization factors (Fig. 6.11a) and a narrow range of shear zone lengths and widths (Figs. 6.11b, c). When considered in the context of the data for the smaller scale shear zones, this suggests that factors other than strain (e.g. location of the shear zones in a network or adjacent to large, competent bodies like pegmatites) may influence strain intensity and localization factors at this scale.

6.6   Summary and Conclusions

Strain localization at the brittle-viscous transition in continental crust is strongly strain- and scale-dependent. This is illustrated in Figure 6.12 with a conceptual model for the evolution of the shear zones at the Cap de Creus. The model is based on a combination of the multiscaling analysis described above with the time-sequence of shear zone development, derived from Fusseis et al. (2006) of the strain gradients across the field area.

Localization may have initiated as shear fractures on one or more scales that correspond to inherited mechanical anisotropies (grey areas in Fig. 6.12): the existing schistosity (millimeter- to centimeter scales), sedimentary layering (decimeter scale) and pegmatite bodies (meter- to 10m scales). Two thresholds were important for the continued evolution of these shear

zones in time and space: (1) the attainment of a critical displacement along individual fractures facilitating viscous creep on these fractures. The onset of creep weakened the shear zone centers, thereby increasing strain rate and driving the lateral propagation of the shear zones, sometimes to lengths beyond the inherited anisotropies. This explains why the scale of some shear zones exceeds that of the existing anisotropies; (2) the attainment of a critical shear zone length and/or viscosity contrast with respect to the country rock, such that the concentrated stress fields at the tips of the encroaching shear zones interacted, thereby causing these shear zones to interconnect (Fig. 6.12b).

The networking of mylonitic shear zones was associated with an upward jump in the scale of the shear zone system and is reflected by the increase in the power-law exponent of localization, Dl. This process of "upscaling" (Handy et al., in press) is contrary to conventional notions of strain localization, in which the deformation is considered to localize at smaller scales than the initial scale(s) of localization. In the case at hand, upscaling is governed by the strain-dependent transition from brittle to viscous deformation on scales from millimeter to hundreds and thousands of meters (Fig. 6.12c). The increase in Dl values from 1 to 2 over this broad range of length scales can therefore be regarded as an empirical growth law for shear zones at the continental BVT.

Systematically varying power-law relationships have also been reported for size/frequency and displacement/length distributions on brittle faults in nature, theory, and experiment (Wojtal 1994, 1996, Nicol et al. 1996, Cladouhos & Marrett 1996, Gross et al. 1997, Ackermann et al. 2001, Hardacre & Cowie 2003). This variance of scaling relationship with scale has been attributed to 1) changes of fault structure (i.e. networking) with strain (Wojtal 1996, Nicol et al. 1996, Gross et al. 1997); 2) changes in deformation mechanisms (Wojtal & Mitra 1986, 1988, Crider & Peacock 2004, and references therein); 3) changes of the mechanical properties of the host rocks and the effective thickness of the mechanical layers encountered during fault growth (Ackermann et al. 2001). We demonstrated that scaling of mylonitic shear zones at the BVT depends on the same processes. An outstanding challenge will therefore be to compare the scaling characteristics of brittle fault populations with the scaling of deep crustal shear zones formed well below the brittle-viscous transition.

6.7 Acknowledgements